Proceedings of ASME Turbo Expo 2011
GT2011
June 6-10, 2011, Vancouver, British Columbia, Canada

GT2011-46413

PERFORMANCE IMPROVEMENT OF TURBOMACHINERY USING PLASMA ACTUATORS

Maria Grazia De Giorgi*
University of Salento
Dep. Engineering for Innovation
Lecce, Italy
mariagrazia.degiorgi@unisalento.it

Stefania Traficante
University of Salento
Dep. Engineering for Innovation
Lecce, Italy
stefania.traficante@unisalento.it

Antonio Ficarella
University of Salento
Dep. Engineering for Innovation
Lecce, Italy
antonio.ficarella@unisalento.it

ABSTRACT

This work deals with the computational modeling of the single dielectric barrier discharge (SDBD) plasma actuator and its applications as a flow actuator. In the literature, plasma actuators have been used especially in order to control boundary layer separation. The plasma acts as a momentum source to the boundary layer allowing it to remain attached throughout a large portion of the airfoil.

The RANS simulations are performed using a CFD code in which the plasma force have been modeled as paraelectric force acting on the charged particles in the working flow

Using this numerical model, different cases have been simulated on NACA 0015 airfoil, depending on the direction of the force, to study the effect of the force on the flow and on the boundary layer.

The best flow control solutions have been displayed when body force component in the direction straight along the flow is positive and the component normal to the flow is considered. Finally, this numerical simulation methodology has been used for the investigations on the potential of plasma actuators, to suppress the flow separation over a compressor blade.

Specifically, the analysis has been focused to evaluate the increasing of the compressor performance depending on the actuator strength and position on the blade.

1. INTRODUCTION

The lift performance of an airfoil is limited by the detachment of the boundary layer from the suction surface. When the chord wise pressure gradient becomes sufficiently large, the boundary layer loses its momentum and separates from the surface. Flow separation is responsible for performance degradation of turbo-machinery and it prevents the design of highly loaded airfoils in turbine and compressors. Successful flow control techniques enable break through improvements in gas turbine performance and design, delaying, reducing, or eliminating completely separation.

A flow control device can be active or passive. The ability to actively manipulate, loosing energy, a flow filed is a characteristic of active flow control.

This paper investigates the potential of plasma actuators to control and to suppress the flow separation over a compressor blade.

Several research projects have been carried out to understand the boundary layer control technologies in compressors. Among them, Merchant [1] and Schuler [2] showed an improvement in pressure ratio while maintaining high efficiencies, considering the control of flow separation by aspiration of the viscous flows that could double the amount of work performed by a compressor stage.

Dang et al. [3] showed numerically that it could be obtained similar performances by an aspirated blade in comparison to a conventional blade, but with a significantly lower solidity.

Culley et al. [4] analyzed the impulsive air injection on a low-speed compressor blade to reattach the boundary layer.

Although the methods presented above have shown interesting results, they have some problems that may inhibit their application in real engines, for example the manufacturing and maintenance cost. These factors stimulate the development of an alternative technology to reduce the flow separation zone on a compressor blade.

The advent of the SDBD (Single Dielectric Barrier Discharge) actuator, based on Electro-Hydro-Dynamic, EHD, model [5-6-7], could provide an interesting alternative. Plasma actuators control the separation of the airfoil surface boundary layer for different applications such as lift augmentation on a wing section, turbine blade separation control [8], turbine tip clearance flow control

[9], drag reduction and noise reduction in fans and compressors [10].

The results from these experiments indicate that several parameters have to be considered for effective flow control. In particular, location of the actuators on the surface, orientation, size and relative placement of the two electrodes, that make up the plasma actuator, applied voltage and frequency of the actuation are the most important parameters to be considered in the analysis.

According to Font [5], Borghi et al.[6], Asada et al.[7], these actuators produce ionization of the flowing air and add localized momentum to the flow through a collision of the moving charged particles with the neutral species of the gas.

EHD phenomena are based on the fact that the currents used are so low that the intensities of the magnetic forces are negligible compared to electric ones. The advantages of this actuators are that they have no moving part, a very short response time and a relatively good efficiency in transforming electrical to mechanical energy.

This work is focused on the moving flow control in the presence of the plasma generated by Dielectric Barrier Discharge. The electro-hydro-dynamic actuator generates plasma (ionized gas) on the boundary layer, a barrier discharge and a moving energy from the electrical field to the neutral species of the gas, where the separation zone is located.

The application of this technology is of considerable interest in the aeronautical field, applied to airfoils and to turbine and compressor blades. Several works [11-24] have investigated the use of plasma actuators on the airfoil, but only few [25-26-27-28] have analyzed the effect of actuator on highly loaded compressors. The focus is therefore to improve the knowledge about the characterization and development of the phenomenon of aerodynamic flow separation on an airfoil in the absence and presence of active type mode control. In particular, this work investigates the ability of a new flow control technology, plasma actuation, to control the separation of the airfoil surface boundary layer in highly-loaded compressors.

2. DIELECTRIC BARRIER DISCHARGE PLASMA ACTUATORS

The plasma and its electric field act as an electric pressure on the fluid: if the electrodes are properly designed, an electric pressure gradient able to slow down or speed up the flow in the unidirectional way can be obtained.

The plasma actuators consists of two electrodes that are separated by a dielectric material (Fig. 1). One of the electrodes is exposed to the air. The other electrode is fully covered by the dielectric material. The electrodes may be excited with a continuous (DC) or with periodic potential difference.

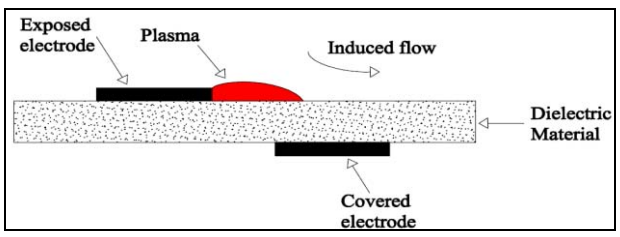

Figure 1. Dielectric Barrier Discharge plasma actuator

In the electric field, ions and electrons are accelerated generating the plasma and then transmit their momentum to the air molecules through collisions. The device produces a homogeneous discharge (plasma) that occupies the space between the electrodes. When the potential difference between the exposed electrode and the dielectric surface is large enough, the air over the dielectric layer ionizes. Ionized air, in presence of electric field, results in body force that acts on neutral air.

The plasma then acts as a "momentum source" to the boundary layer that remains attached to a larger portion of the surface.

The process of ionizing the air in this configuration is classically known as a single dielectric barrier discharge (SDBD) [29]

Efforts to address the paraelctric flow (EHD) mechanism of DBDs on fluid flows, is undertaken by Roth et al. [30-31-32-33].

In this work to account for the body force term, depending on the electrical field produced by the plasma actuator and acting on the fluid, a numerical model has been used, based on a simple expression for the body force to represent the plasma effect on the fluid [20].

A schematic representation of the plasma region is shown in Fig. 2, where the triangular region OAB represents the plasma formation zone and doesn't include the strong electric field curvature near the electrode edge regions. So, as reported by Jayaraman and Shyy in [20], the field variation in space can be linearized without computing the detailed electric field. In particular, the field lines are such that the field strength decreases as one moves far away from the source.

The variation of the E in the linear field model can be written as

$$|\vec{E}| = E_0 - k_1 x - k_2 y \tag{3}$$

where E_0 is the electric field in the darkened region on OB in Fig. 2, k_1 and k_2 are two positive constants which represent the gradient of electric field intensity along the two mutually perpendicular directions, x (OB) and y (OA). The sign of these two constants ensures that the electric field intensity decreases as one move along the positive directions of the axes [6].

In the equation (3) E_0 can be written as

$$E_0 = V/d \tag{4}$$

where d is the distance of separation between the two electrodes in the x direction and V is the applied voltage potential.

The constants *k1* and *k2* are evaluated by using the condition that the field strength is the breakdown value at the plasma-fluid boundary.

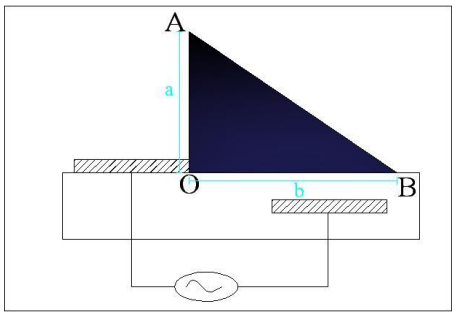

Figure 2. Schematic illustrating of the linear plasma field model

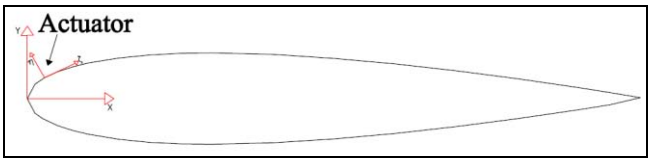

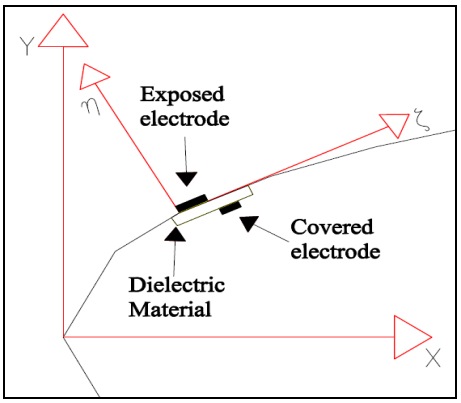

Figure 3 . ξ - η coordinate system located near leading edge- enlarged view

The electric field is then obtained from

$$E = \frac{|E|}{\sqrt{k_1^2+k_2^2}}\left\{k_\xi k_2 \hat{\xi} + k_\eta k_1 \hat{\eta}\right\} \quad (5)$$

where ξ and η are unit vectors respectively along and normal to the exposed electrode (Fig 3). For the airfoil, this coordinate system is located at the tangent to the surface at the leading edge of the electrode, as represented in Fig. 3. The orientation is adjusted by choosing k_ξ and k_η [7].

The time period is Δt during which the plasma is formed. The body force components along the x and y direction are [8]:

$$f_x = E_x \rho_c e_c \quad (6)$$

$$f_y = E_y \rho_c e_c \quad (7)$$

This force acts only in the regions where the plasma is present. The delta function ensures this restriction, because is equal to one into the triangular region OAB and is equal to zero outside.

The effective force is given by

$$f_{effx} = \alpha f_x \delta_x \quad (8)$$

$$f_{effy} = \alpha f_y \delta_y \quad (9)$$

where α is a factor to account for the collision efficiency.

The force can be averaged over a time:

$$F_{tavex} = f_{effx} \Delta t / T_t \quad (10)$$

$$F_{tavey} = f_{effy} \Delta t / T_t \quad (11)$$

where T_t is the period of the applied voltage

Then, the body force components can be written as:

$$F_{tavex} = \theta f_{effx} \Delta t \quad (12)$$

$$F_{tavey} = \theta f_{effy} \Delta t \quad (13)$$

where θ (reciprocal of T_t) is the frequency of the applied voltage. The F_{tavex} and F_{tavey} are the body force components, f_{bx} and f_{by} , in the Navier-Stokes equations, as explained in the next section.

3. FLUID DYNAMIC GOVERNING EQUATIONS

The governing model equations are Reynolds averaged Navier-Stokes (RANS) equations. For this case the equations for conservation of mass and momentum have the form:

$$\frac{\partial \rho}{\partial t} + \nabla \cdot (\rho \vec{v}) \quad (1)$$

$$\frac{\partial}{\partial t}(\rho \vec{v}) + \nabla \cdot (\rho \vec{v}\vec{v}) = -\nabla p + \nabla \cdot (\bar{\bar{\tau}}) + \rho \vec{g} + \overrightarrow{f_b} \quad (2)$$

where p is the static pressure, $\bar{\bar{\tau}}$ is the stress tensor, v is the velocity, ρ is the flow density, ρg and $\overrightarrow{f_b}$ are the gravitational body force and external body force, respectively.

As mentioned above, the external body force, added to the momentum equation, represents the effect of the plasma actuator on the fluid flow.

The F_{tavex} and F_{tavey}, given from the equations (12) and (13), have a value of zero in a region where we do not have the plasma and take the following for under the influence of the plasma:

$$F_{tave} = \theta \alpha E \rho_c e_c \delta \Delta t \quad (14)$$

$$\overline{E} = \left(\frac{E k_2}{\sqrt{k_1^2+k_2^2}}, \frac{E k_1}{\sqrt{k_1^2+k_2^2}}\right) \quad (15)$$

In this study, to analyze the effects of the plasma actuator on the boundary layer separation of the airfoil, the paraelectric EHD body force of DBD plasma actuators has been simulated by the ANSYS Fluent 12.0 code with user defined routines.

4. PLASMA EFFECTS ON THE NACA 0015

4.1 NACA 0015: Computational domain and boundary conditions

First numerical simulations have been performed on an airfoil 2D NACA 0015 with a chord length equal to 0.2 m, in steady RANS. It was used a structured C-type grid that was generated using the software GAMBIT 2.0.

The size of the computational domain was chosen in order to obtain a domain- independent solution. The dimension of the domain is inspired by B. Schmutz [34], Orlov et al. [16] and Jayaraman et al. [17]. Schmutz indicates that the dimensions of the computational domain should be at least 3 airfoil chord in front of the airfoil and 5 chord behind. So, in this work the inlet boundary was located 8.6 chord lengths from the airfoil leading edge, and the outflow boundary was located 9.45 chord lengths downstream the airfoil trailing edge, not to affecting the computational cost of the simulation

The grid consists of 400x100 points (Fig. 4). The minimal size of the grid is 1 x 10^{-5} chord lengths. The maximum y^+ value is 0.4. The quality of the grid is defined by maximum cell squish equal to 0.99 and maximum aspect ratio equal to $1.75e^5$.

A pressure based solver has been used. Pressure far-field conditions are used to model the free-stream condition at infinity. The pressure far-field boundary condition is a non-reflecting boundary condition based on the introduction of Riemann invariants for a one-dimensional flow normal to the boundary.

The k-ε turbulence model, which presents the advantage that it doesn't need excessive computational times, has been used. The enhanced wall treatment has been considered for the near wall model approach, where the mesh is very fine close to the wall and the conditions are solved all the way to the wall.

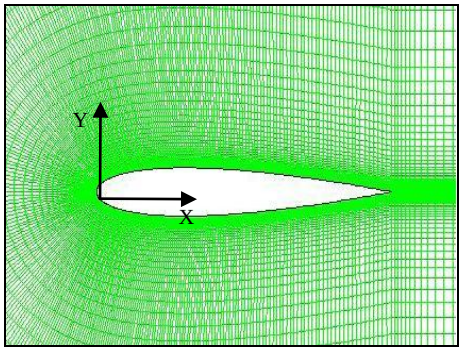

Figure 4. C-type structured mesh

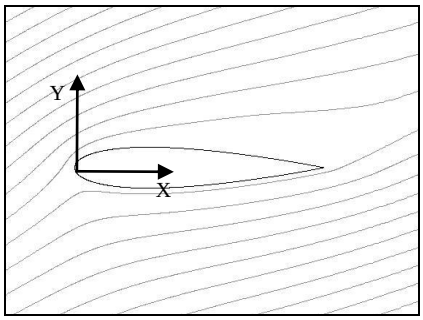

Figure 5. Streamlines contours without plasma actuator

4.2. Plasma effects as constant local body force: results and discussion

First, the flow with no plasma actuators is simulated and the streamlines contour is shown in Fig. 5 where a large separation zone could be observed at 21% chord.

Then, different virtual EHD body force fields are incorporated into the Navier-Stokes equations to show body force field effects on the wing surface. Among all active flow control methods, EHD method operates on the basis of body force induction on flow field. The effects of different body force fields on three domains are studied to reduce the separation zone on the NACA 0015 profile. First, a constant body force field, applied in different regions close to the airfoil, has been simulated to study the effects on flow separation zone. The inflow was set at 35 m/s, the Reynolds number is equal to 438000 and Mach number is 0.1. The angle of attack was set at 23 degrees. The turbulence intensity of the inflow was set to 10%.

Considering the body force field as constant around the airfoil, three different domains (Fig. 6) CEFDC, GABHG and GAILG, are used as body force field acting domains, with different strengths in different directions [19]. As reported by Boeuf et al. [35] the estimation of the force per unit volume, on a DBD surface for flow control applications, would be in the (10^2 – 10^4) N/m^3 range. So it's reasonable to consider body force field strength from 100 Nm^{-3} to 30.000 Nm^{-3} in the next simulations.

First, selecting the CEFDC domain and implementing body force with different strengths 1000-10000 Nm^{-3} in the x direction, the separation point moves rearward. For f_b =10000 Nm^{-3} not only the separation zone vanishes completely , but also the streamlines over the pressure surface adapt better than the streamlines related to the different body force values to the airfoil profile (Fig. 7). This procedure is also shown in Fig. 8 by the pressure coefficient distribution along the airfoil chord line. In particular, in Fig. 9 it is shown that for f_b =10000 Nm^{-3} the pressure coefficient value becomes smaller than the other values on the pressure side, that leads to lift augmentation.

Body force in the lower region of the airfoil is not effective in separation control so a deep analysis has been done on the upper region of the airfoil. The GABHG domain is used to analyze the body force effect in the –y direction.

Looking to the pressure coefficient Cp distribution, increasing the body force up to f_b = 30000 Nm^{-3}, the minimum value on the pressure side of the airfoil increases, reducing the lift, and the separation point moves to 22% chord (Fig. 10).

According to the results mentioned above, it is considered the GABHG domain restricts to the GAILG area with different body force strengths 100 Nm^{-3} - 20000 Nm^{-3} in the x direction, like CEFDC conditions.

For f_b =10000 Nm^{-3} the separation point moves reaward and for f_b =20000 Nm^{-3} it moves from 21% (without plasma) to 63% chord length. As shown in Fig. 11 the minimum values of pressure coefficient on the pressure

side becomes 1.5 smaller than the plasma-off value, increasing the lift.

Figure 12 shows the comparison between the pressure coefficient distributions for different domains and the same body force f_b = 10000 Nm^{-3}. It is evident that the best solutions are obtained by CEFDC and GAILG domains simulations.

According to [5] and to the simulation results discussed above:

- The most effective plasma actuator is one that induces the best body force field corresponding to our application;
- Only body force with a strength of more than 1000 Nm^{-3} could affect the flow;
- The best direction for acting body forces is the x direction, parallel to the chord line.

Figure 6. Schemating of acting domains

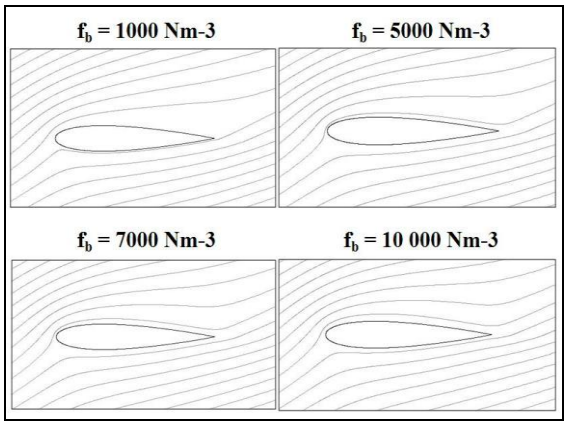

Figure 7. Streamlines contours, different constant body force f_b in the CEFDC domain

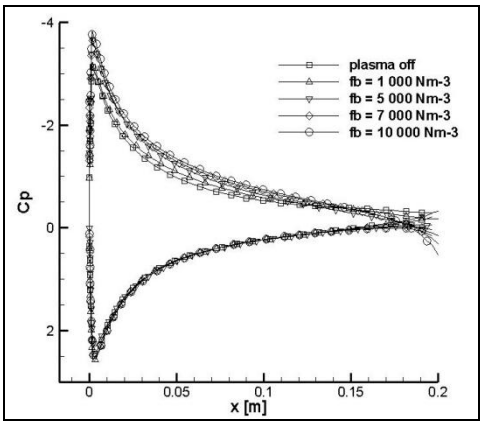

Figure 8. Pressure coefficient distributions, different constant body force f_b in the CEFDC domain

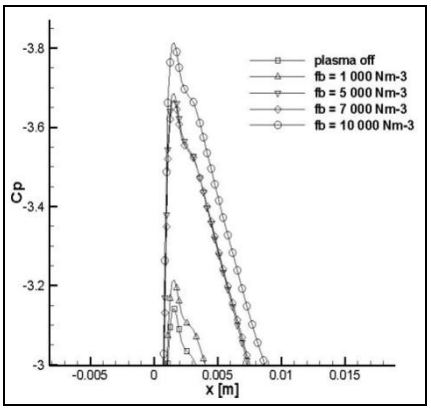

Figure 9. Enlarged view of pressure coefficient distributions, different constant body force f_b in the CEFDC domain

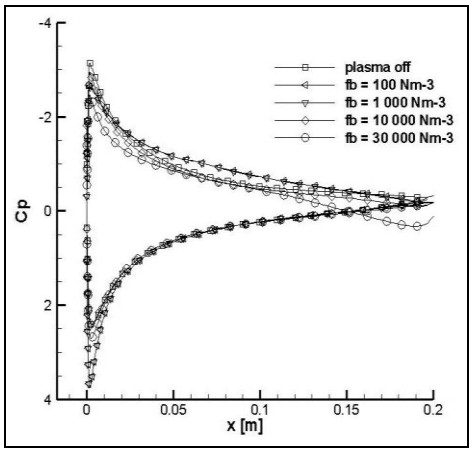

Figure 10. Pressure coefficient distributions, different constant body force f_b in the GABHG domain

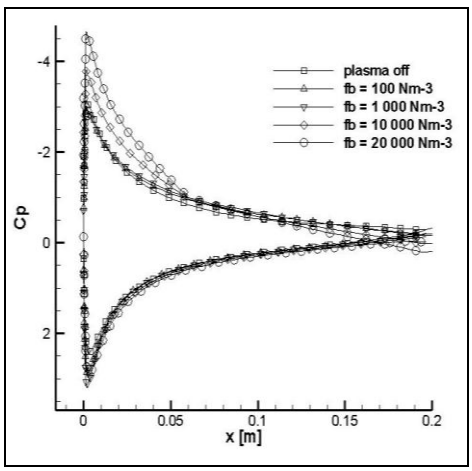

Figure 11. Pressure coefficient distributions for different constant body force f_b in the GAILG domain

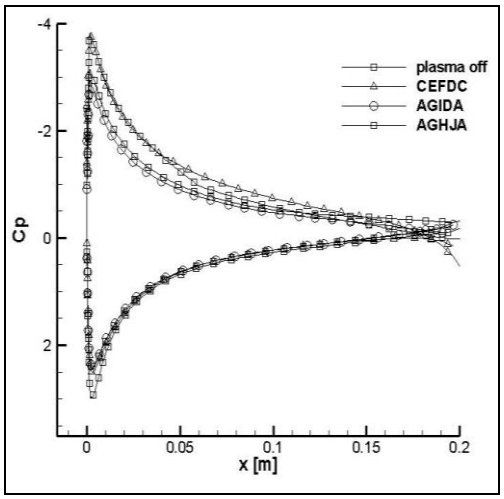

Figure 12. Pressure coefficient distributions for a constant body force f_b = 10000 Nm-3 in the different domains

4.3. Plasma effect as electric force field

After considering plasma effects as local body force, so neglecting the electric field, in order to simulate the plasma effects as a variable body force, depending on the applied electric field, the same values of parameters used in the experiments [30-31] have been considered.

Then, the results have been validated with the data reported in R. Sosa and G. Artana [18].

The inflow was set at 1.44 m/s with the Reynolds number Re = 18000. The angle of attack was set at 15°. The turbulence intensity of the inflow was set to 10%. In this test case the plasma actuator and then the force is applied at 2.8% of the chord length.

Numerical model validation

The numerical model described above has been validate by the simulations of the EHD actuator effects on a moving flow on a NACA 0015, studied experimentally by R. Sosa and G. Artana [18] .

The airfoil is NACA 0015 with a chord length equal to 200 mm, an actuator is located on the suction surface. In the experiments a copper wire of 0.9 mm diameter was fitted in a slot of the airfoil surface at x/c = 0.55. The plate electrode is located at x/c = 0.79. The first electrode is the lower electrode, the second is the upper electrode. The distance between the two electrodes is equal to 37 mm.

The force components Fx and Fy have been calculated and simulated with the CFD code, considering the applied voltage of 30 kV, the flow velocity of 1.44 m/s and the airfoil with an angle of attack equal to 15°.

Fy component has been considered in the negative direction –y, normal to chord of the airfoil and oriented in the lower surface, because strength of the body force decreases as one moves far away from the plasma region.

The pressure coefficient Cp distribution obtained in the experiments by [18] and by the predicted profiles are compared in the Fig. 13.

The distribution without plasma obtained by CFD simulations is similar to one in the experimental case. The results obtained from the simulation and experimental test were not so close for this case. So, the difference can be explained by the uncertainty of the measurement instruments and the angle of attack equal to 15°, greater than angle of attack reported by [18].

On the other hand, to analyze the plasma effect, the best pressure coefficient Cp distribution, resulted by the simulations, is obtained by the Eq. 14 calculated with θ = 1kHz and $\Delta t = 3\mu s$.

Considering the plasma actuator effects, the results obtained from simulation and experimental test were very close. Good agreement is evident comparing the predicted pathlines and experimental observations (see Fig. 14 and Fig. 15). Numerical data and experimental observations show that even in the region of the trailing edge, the flow remained attached. When actuator is operated the reattachment of the flow takes place and the streamlines then contoured the model indicating a full reattachment of the flow.

Plasma effects as electric force field: results and discussion

Using the previous numerical model, a user defined function has been implemented to model the body force depending on the electric field. As shown in Fig.16 the body force components are located at the x,y coordinate system (x coordinate is along the chord of the airfoil and y coordinate is normal to x), but calculated regarding ξ , η. system, located at the tangent to surface at the leading edge of the electrode.

In the local coordinate system ξ , η, four orientations (Fig. 16) are considered, corresponding to $k\xi$ and $k\eta$ pairs of:

- case 1 {1,1},
- case 2{1,-1} (vertical force component reversed),
- case 3{0, 1} (normal to body and away from it),
- case 4 {0, -1} (normal to body and towards it).

The parameters θ = 1 kHz, Δt = 3 μs, α = 1, $\rho_c = 10^{11}$, V = 5.65 kV, used to calculate Fx and Fy components from Eq. (14), were considered in the experimental cases by [22-30-31].

The position of the actuator and its geometry are defined according to [23] and [24],

Assuming "a" and "b" parameters (Fig. 2) as indicated in the formulation of [18], the force is applied at 2.8% chord length, slightly downstream of the initiation of separation.

According to "b" value, a computational domain along x and y coordinates are calculated.

The parameter k_1 is calculated from Eq. (3) and set to 5.82 kV/cm^2. Similarly, k_2 = 7.70 kV/cm^2.

E_0, the maximum electric field in the plasma region is obtained from Eq. (4):

$$E_0 = V/d = 7.915 \text{ kV/cm}$$

The electric field is given by Eq. (15):

$$Ex\ (x,y) = 0.79\ E$$
$$Ey\ (x,y) = 0.6\ E$$

According the "a" and "b" values and the Eq. (12) and Eq. (13), the force components are equal to:

$$Fx = 3.83 \times 10^{-8}\ E$$
$$Fy = 2.89 \times 10^{-8}\ E$$

where *E* has the unit of V/cm.

As mentioned above, the electric field is calculated along the ξ , η local coordinate system, from the Eq. (5).

According to the four orientations, in the x, y coordinate system, the Fx component values is positive or zero along the x direction, while the Fy is along the y or –y direction.

According to the experiments [18], the applied voltage is equal to 30 kV and the flow velocity value is 1,44 m/s. As mentioned above the flow separates around 2.8% chord length, so the simulations are performed with angle of attack equal to 15°, greater than angle of attack reported by [18]. According to airfoil and Reynolds number and inspired by literature, 15° is defined as critical angle of attack for the airfoil stall.

In Fig. 17 the pressure coefficient profiles shows that the best performance is case 1 because the pressure coefficient decreases on the pressure side.

According to Fig. 18 the best performance is evident in case 1 and case 2 because the separation zone moves from 21% to 43% of the chord length. This is confirmed by the velocity contours solution (Fig. 19).

In any experimental application of the case, the geometry of the actuator must be considered, identifying the values of a, which represents the highest value of electric field along y and of the electric force at the upper electrode, and b, that is not exposed electrode length and the distance between the two electrodes.

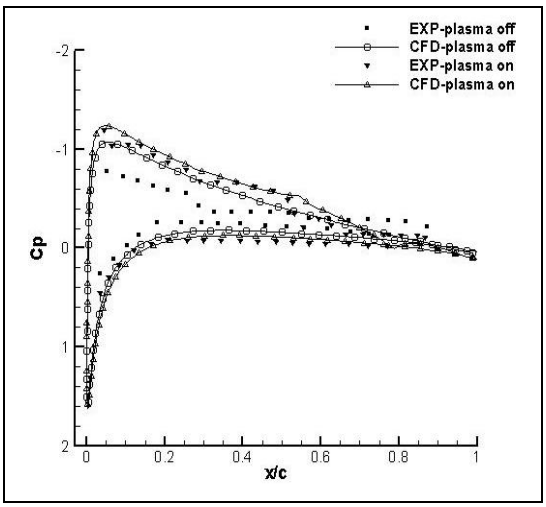

Figure 13. Pressure coefficient distributions with and without plasma (CFD θ=1kHz, Δt=3 μs; experimental [18])

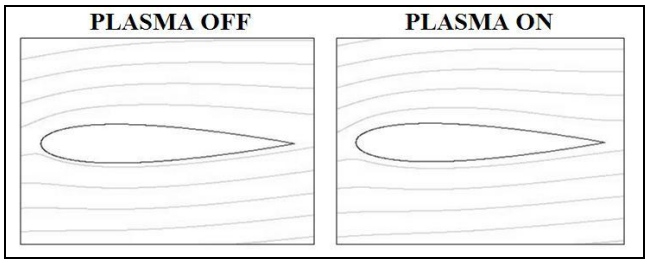

Figure 14. Streamlines contours, CFD results with (right) and without (left) plasma (α= 15°, θ=1kHz, Δt=3 μs)

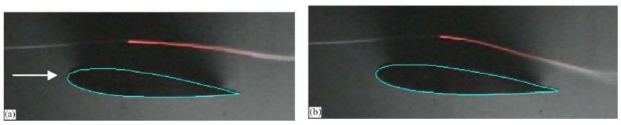

Figure 15. Streamlines, experimental [9] plasma off (a) plasma on (b) (Re= 15.000, α= 5.8°)

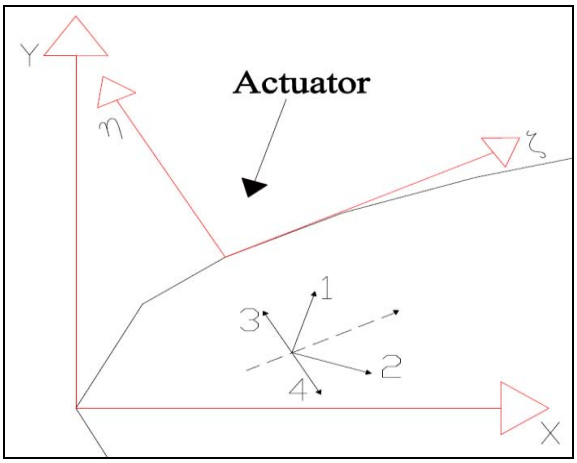

Figure 16. Body force field configurations for numerical approach

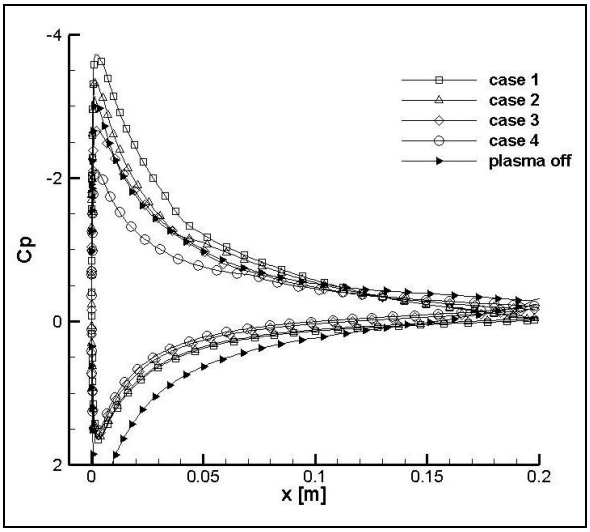

Figure 17. Pressure coefficient distributions, at different body force directions

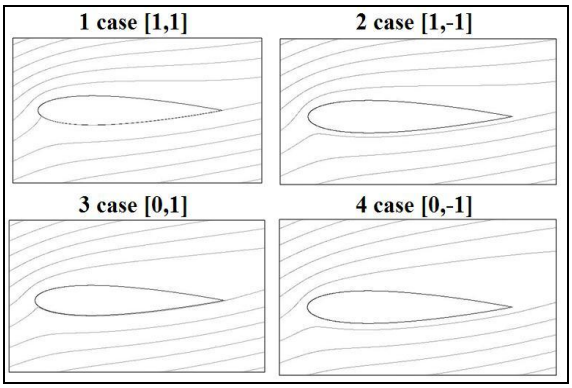

Figure 18. Predicted flow streamlines at different body force directions

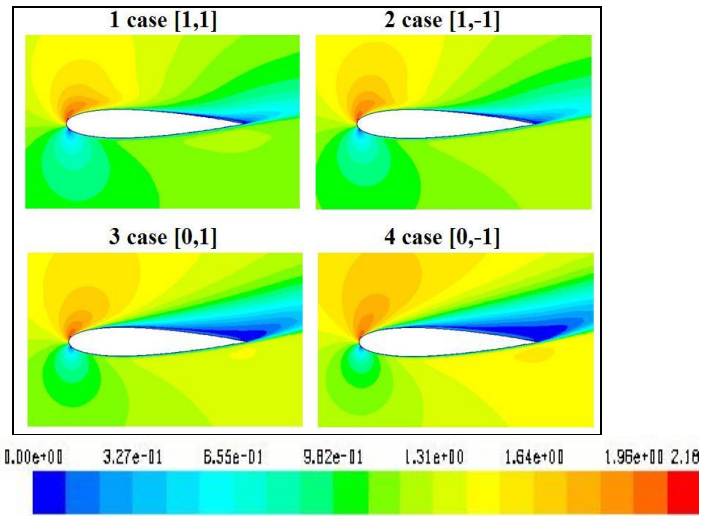

Figure 19. Velocity contours, at different body force directions

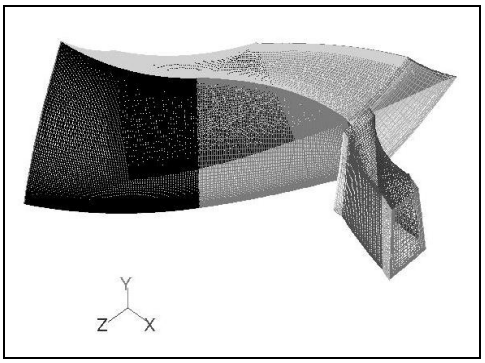

Figure 20: Axial compressor mesh

5. PLASMA ACTUATOR ON AXIAL COMPRESSOR

Finally, to evaluate the effectiveness of plasma actuator and to prevent flow separation, numerical simulations concerning a stage (rotor-stator) of an axial compressor with plasma actuators on the rotor suction blade surface have been implemented.

5.1 Axial compressor: computational domain and boundary conditions

The simulations reported in this paper are based on a transonic axial flow compressor, which specifications are summarized in table 1.

Table 1. Parameters of axial compressor

Rotational speed (rpm)	37500
Mass flow rate (kg/s)	4
Rotor blade number	16
Stator blade number	40
Blade rotor axial chord (m)	0.033
Tip radius (m)	0.042
Hub radius (m)	0.3
Inlet total pressure (Pa)	101325
Inlet total temperature (K)	288

The axial compressor has two blade rows: the first row is the rotor, with 16 blades, which is operating at a rotational speed of 37500 rpm and revolves about the negative x-axis. The second row is the stator with 40 blades. Only a portion of the geometry (two rotor blades and two stator blades) has been modelled.

Since the periodic angles for the rotor and stator are different, a mixing plane has been used at the interface. The mixing plane is defined at the rotor outlet/stator inlet. The mesh is set up with periodic boundaries on either side of the rotor and stator blades. A pressure inlet is used at the upstream boundary and a pressure outlet at the downstream boundary.

The mesh, shown in the Fig. 20, is characterized by 1152420 cells, 3511822 faces, 1224482 nodes along the 3 axes: x, y and z. The quality of the grid is defined by maximum cell squish equal to 0.91 and maximum aspect ratio equal to $2.25e^{1}$. The maximum y^{+} value is 20-60 .

The inlet boundary conditions consist of a constant total pressure and a 5% of turbulence intensity . The outlet conditions are the turbulence intensity and ratio set to 5% and 10, respectively, and the radial equilibrium pressure distribution. A density based solver and k-ε turbulence model have been used. The flow is transonic and the Mach number is equal to 1.1.

5.2 Axial compressor: results and discussions

The results obtained by the simulations, carried out on NACA 0015 airfoil, can be useful for an application to the turbo-machinery blades, and in particular to the compressor and fan blades. The aerodynamic performance of compressors and fans is essentially measured in terms of pressure ratio and efficiency. So, when the suction surface boundary layer separates, the pressure ratio and efficiency decrease rapidly. To control, adding momentum, the separation of the airfoil surface boundary layer in compressors, a plasma actuator will be considered.

The numerical study of the compressor have been done with continuous actuation to evaluate the increasing of the compressor performance depending on the actuator strength and the position on the blade.

First, eighteen simulations, depending on the plasma actuator force value and the position of the actuator, that is

located on the blade suction, are carried out.

The three actuator positions (Fig. 21) are [12]:

- position 1: just upstream the separation zone;
- position 2: at the beginning of the separation zone, inside it;
- position 3: at the point where the flow begins to slow down on the suction side.

For each actuator location, different actuator strengths are studied: 581 N/m^3, 1938 N/m^3, 3876 N/m^3 , 7752 N/m^3, 10000 N/m^3 and 17442 N/m^3 that corresponding to 0.3 N/m, 1N/m, 2N/m, 4N/m, 5.16 N/m and 9 N/m, respectively.

To evaluate the performance of the compressor, pressure ratio and efficiency over the whole stage of the axial compressor are considered in this analyses.

The actuator position is important to define the power that must be submitted to the actuator. At position 1 and 2 the fluid velocity is decreased because of the recirculation zone, while at position 3 the flow decelerates but its velocity is still important. So, the actuator must impart momentum to a larger amount of fluid than at position 1 and 2.

However the actuator positions 1 and 2 are more effective than position 3 from energy point of view, the compressor blades are thin near their trailing edge, then position 3 offers a better location to integrate the plasma actuator on the airfoil.

The optimal location could be a compromise between energy and geometrical considerations.

According to numerical simulation results (Fig. 22), the effect of the actuator position is visible for the lower body forces. In addition, for the actuator strength equal to 0.3 N/m the pressure ratio value is equal to one related to F = 1N/m.

However, the effect of the actuator location on the rotor blade is insignificant for body force values higher than 4 N/m . So, the plasma actuator and its electrodes could be located everywhere over airfoil, according to the geometry parameters of the airfoil.

For these reasons, the results are reported only for different actuator strengths and not for the actuator position.

The simulations were carried out at an incident angle of 0°. As shown in the Fig. 22 and Fig. 23, the actuator strength has a significant impact on pressure ratio and efficiency. This parameters vary linearly with actuator strength.

According to Gang et al [28], who investigated experimentally the influence of plasma actuators as an internal flow separation control device in a set of compressor cascade, increasing the actuator strength from 0 N/m to 4 N/m, the turbulence intensity decreases in presence of the plasma actuation , as shown in Fig. 24 and Fig. 25. In fact, a smaller turbulent intensity value for F = 9 N/m, compared to one without plasma, explains the flow separation decreasing (Fig. 26).

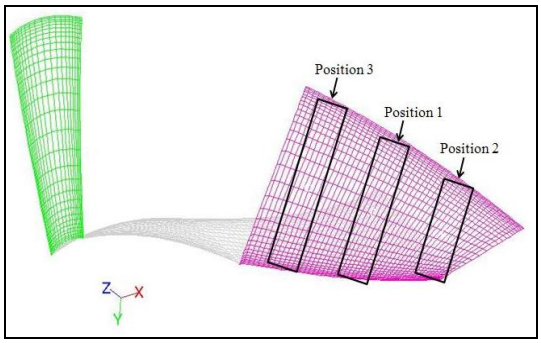

Figure 21. The positions at which plasma actuators are positioned on the rotor suction blade (rotor blade is pink, rotor inlet is green)

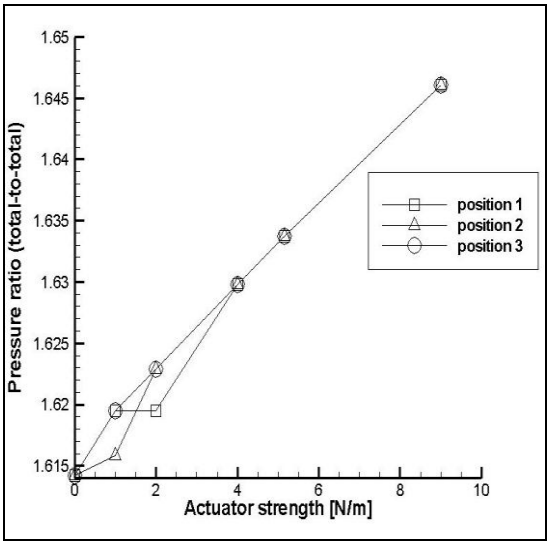

Figure 22. Effect of actuator strength on pressure ratio for different actuator location

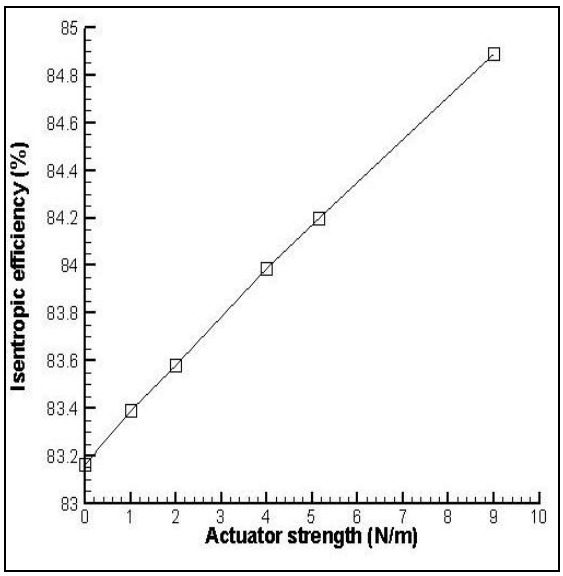

Figure 23. Effect of actuator strength on isentropic efficiency

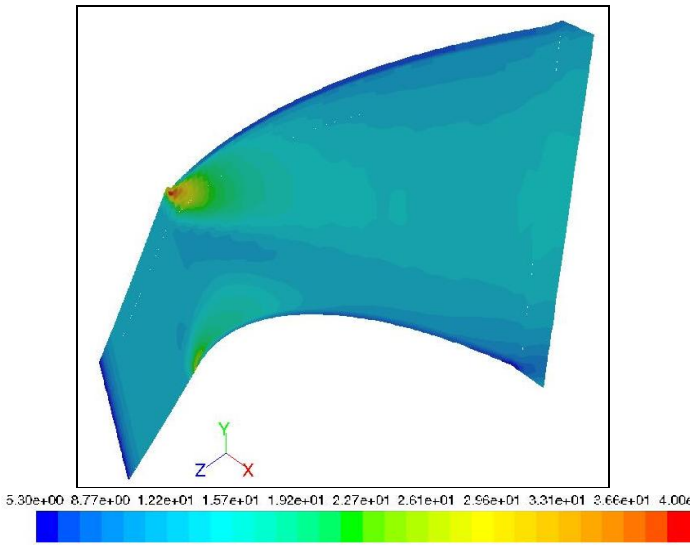

Figure 24. Turbulence intensity contour without plasma (midspan plane)

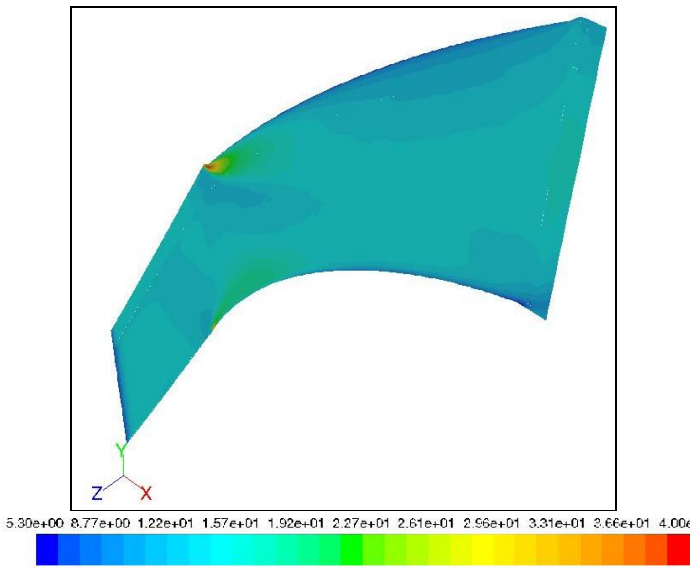

Figure 25. Turbulence intensity contour with F = 9 N/m (midspan plane)

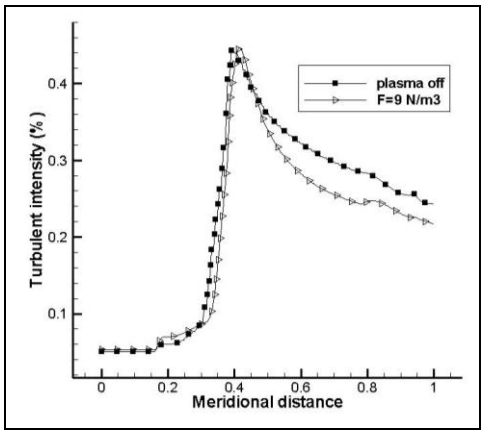

Figure 26. Turbulence intensity (midspan plane)

6. CONCLUSION

The focus of this study is the analysis of the response of a separated flow field to body forces arising from suitably placed dielectric barrier discharge actuator in order to avoid flow separation.

First, the plasma body force has been considered as a localized constant force and applied at three different domains close to the airfoil. The simulation results show that forces strength higher than 1000 Nm^{-3} can affect the flow and that the best direction for the forces is the chord wise direction.

Then, a numerical model was implemented to simulate the different components of the forces due to the electric field generated at the plasma region. After a first phase of validation, this numerical model has been implemented to analyze the effect of the force direction on the moving flow.

The results show a good control of the flow on the surface in presence of plasma actuator, and in particular, the best solution is case 1 (Fig. 16), because the pressure coefficient decreases on the pressure side compared to case without plasma too. The plasma formation is more in the region closest to the inner edges of the two electrodes and, in particular, in this case, the directions of the body force components define a body force pointed away from airfoil and decreased in magnitude as one moves away from plasma formation region.

Finally, the previous numerical approach has been used for the investigations on the potential application of plasma actuators to suppress the flow separation over a compressor blade, in order to increase its pressure ratio, efficiency and power on a compressor blade suction side, to suppress boundary layer separation, to increase axial compressor performance and flow turning. In particular the analysis was focused to evaluate the effect of actuator strength and position on the blade, and the effect on the performance increase of the compressor. Results show a major impact of the actuator strength on the performance increase of the compressor.

According to numerical results, the optimal actuator location could be a compromise between energy and geometrical considerations, but, in this work, the plasma actuator position doesn't influence the effect on the flow field. So, the analysis is focused on the effect of the actuator strength on the flow separation. Simulations show that plasma actuator can increase the pressure ratio, efficiency, and power imparted by the rotor to the air and that the pressure ratio, efficiency and rotor power increase almost linearly with actuator strength.

Increasing the actuator strength leads to reduce turbulent intensity value and the flow separation, as indicated by results with body force equal to 9 N/m.

NOMENCLATURE

EHD	Electro-Hydro-Dynamic
Cp	Pressure coefficient
P	Density, kg/m^3

V	Velocity, m/s
p	Static pressure, Pa
T_t	Period for the applied voltage, 1/kHz
θ	Frequency, kHz
Fb	Exetrnal body force, N m^{-3}
T	Stress tensor
E_0	Electric field max in the plasma region, kV/cm
k1, k2	Constants, kV/cm^2
V	Applied voltage, kV
D	Distance between electrodes, cm
H	Unit vector normal to the exposed electrode
Ξ	Unit vector along the exposed electrode
G	Gravity acceleration, m s^{-2}
ρ_c	Electron density, cm^{-3}
e_c	Electron charge, C
α	Collision efficiency
Δ	To define the plasma region
Δt	Period time to generate plasma, μs

REFERENCES

[1] Merchant, A., Kerrebrock, J.L., Adamczyk, J.J., and Braunscheidel, E., 2005. "Experimental investigation of a high pressure ratio aspirated fan stage", ASME Journal of Turbomachinery, 127 (1), pp. 43-51.

[2] Schuler, B.J., Kerrebrock, J.L., and Merchant, A., 2005. "Experimental investigation of a transonic aspirated compressor", ASME Journal of Turbomachinery, 127 (2), pp. 340-348.

[3] Dang, T.Q., Van Rooij, M., and Larosiliere, L.M., 2003. "Design of aspirated compressor blades using thre-dimensional inverse method", Tech. Rep. NASA TM-2003-212212, NASA Glenn Research Center, Cleveland, Ohio.

[4] Culley, D.E., Braunscheidel, E.P., and Bright, M.M., 2003. " Impulsive injection for compressor stator separation control", Tech. Rep. NASA TM-2003-213859, NASA Glenn Research Center, Cleveland, Ohio.

[5] Font, G.I., 2004. "Boundary layer control with atmospheric plasma discharges", 40th AIAA Joint Propulsion Conference, Fort Lauderdale, Florida.

[6] Borghi, C. A., Cristofolini, A., Neretti, G., 2009. "Interazione elettroidrodinamica indotta da scarica a barriera", XXV Riunione Annuale dei Ricercatori di Elettrotecnica.

[7] Asada, K., Ninomiya, Y., Oyama, A., Fujii, K., 2009. "Airfoil flow experiment on the duty cycle of DBD plasma actuator" 47th AIAA Aerospace Sciences Meeting, Orlando, Florida.

[8] Huang, J., Corke, T.C., and Thomas, E.O., 2006. " Unsteady plasma actuators for separation control of low-pressure turbine blades", AIAA Journal, 44 (7), pp. 267-278.

[9] Morris, S.C., Corke, T.C., VanNess, D., Stephens, J., and Douvillet, T., 2005. "Tip clearance control using plasma actuators", Proceedings of the 43rd AIAA Aerospace Science Meeting and Exhibit, Reno, Nevada, pp. 14069-14076.

[10] Lemire, S., and Vo, H.D., 2008. "Reduction of fan and compressor wake defect using plasma actuation for tonal noise reduction", Proceedings of the ASME Turbo Expo, Berlin, 6, pp. 837-848.

[11] Fu. X., Li, Y., Li, B., and Kwok, D.Y., 2009. "Drag force reduction on an airfoil via glow discharge plasma-based control", The European Physical Journal – Special Topics, 171 (1), pp.195-204.

[12] Asada, K., Ninomiya, Y., Oyama, A., and Fujii, K., 2009. "Airfoil flow experiment on the duty cycle of DBD plasma actuator" 47th AIAA Aerospace sciences meeting, Orlando, Florida.

[13] Benard, N., Jolibois, J., and Moreau, E., 2009. "Lift and drag performances of an axisymmetric airfoil controlled by plasma actuator", Journal of Electrostatics, 67, pp. 133-139.

[14] Opaits, D.F., Roupassov, D.V., Starikovskaia, S.M., Starikovskii, A.Yu., Zavialov, I.N., Aand Saddoughi, s.g., 2005. "Plasma control of boundary layer using low-temperature non-equilibrium plasma of gas discharge", AIAA Paper.

[15] Rafika, M., Ramzi, H., and Sassi, B.N., 2009. "A study of DC surafce plasma discharge in absence of free air flow:ionic wind velocity profile", Journal of Applied Fluid Mechanics, 2 (2), pp. 43-48.

[16] Orlov, D.M., Apker, T., He, C., Othman, H., and Corke, T.C., 2007. "Modeling and experiment of leading edge separation control using SDBD plasma actuators", 45th AIAA Aerospace Sciences Meeting and Exhibit, Reno, Nevada.

[17] Jayaraman, B., Lian, Y., Shyy, W., 2007. "Low reynolds number flow control using dielectric barrier discharge actuators", 37th AIAA FluidDynamics Conference and Exhibit, Miami, Florida.

[18] Sosa, R., Artana, G., 2006. "Steady control of laminar separation over airfoils with plasma sheet actuators", Journal of Electrostatics, 64, pp. 604-610.

[19] Abdoli, A., Mirzaee, I., Anvari, A., Purmahmod, N., 2008. "Simulation of body force field effects on airfoil separation control and optimization of plasma actuator", Journal of Applied Physics, 41 (17), pp. 1-9.

[20] Jayaraman, B., and Shyy, W. 2008. "Modeling of dielectric barrier discharge-induced fluid dynamics and heat transfer" Progress in Aerospace Sciences, 44 (3), pp. 139-191.

[21] Gaitonde, D.V., Visbal, M.R., Roy, S., 2005. "Control of flow past a wing section with plasma-based body forces", 36th AIAA Plasmadynamics and Lasers Conference, Toronto, Canada.

[22] Shyy, W., Jayaraman, B., Anderssonb, A., 2002. "Modeling of glow discharge-induced fluid dynamics", Journal of Applied Physics, 92, pp. 6434-6443.

[23] Forte, M., Jolibois, J., Pons, J., Moreau, E., Touchard, G., Cazalens, M., 2007. « Optimization of a dielectric barrier discharge actuator by stationary and non-stationary measurements of the induced flow velocity :application to airflow control", Experiments in Fluids, 43 (6), pp. 917-928.

[24] Jolibois, J., Forte, M., Moreau, E., 2008. " Application of an AC barrier discharge actuator to control airflow separation above a NACA 0015 airfoil :optimization of the actuation location along the

chord", Journal of Electrostatics, 66, pp. 496-563.

[25] Lemire, S., Duc Vo, H., Benner, W., 2009. "Performance improvement of axial compressors and fans with plasma actuation", International Journal of Rotating Machinery.

[26] Lemire, S., and Duc Vo, H., 2011. "Reduction of fan and compressor wake defect using plasma actuation for tonal noise reduction", Journal of Turbomachinery, 133.

[27] Li, Y., Wu, Y., Zhou, M., Su, C., Zhang, X., and Zhu, J., 2009. "Control of the corner separation in a compressor cascade by steady and unsteady plasma aerodynamic actuation", Experiments in fluids, 48 (6), pp. 1015-1023.

[28] Gang, L., Chaoqun, N., Yiming, L., Junqiang, Z., and Yanji, X., 2008. "Experimental investigation of flow separation control using dielectric barrier discharge plasma actuators", Plasma Science and Technologies, 10 (5), pp. 605-611.

[29] Corke, T.C., Post, M.L., and Orlov, D.M., 2008. " Single-dielectric barrier discharge plasma enhanced aerodynamics: concepts, optimization and applications". Journal of propulsion and power, 24 (5), pp. 935-945.

[30] Roth, J.R., Sherman, D.M., and Wilkinson, S.P., 1998. "Boundary layer flow control with a one atmosphere uniform glow discharge", 36th AIAA Aerospace sciences meeting, Reno, Nevada.

[31] Roth J. R., Sherman D. M. and Wilkinson S. P., 2000. "Electrohydrodynamic Flow Control with a Glow Discharge Surface Plasma", AIAA Journal, 38 (7), pp 1166-1172.

[32] Roth, J.R., 1995. "Industrial plasma engineering: Vol.I – Principles", Institute of Physics, Bristol.

[33] Roth, J.R., 1998. "Electrohydrodynamically induced airflow in a one atmosphere uniform glow discharge surface plasma", 6P-67, Proceedings of the 25th IEEE international conference on plasma science, Raleigh, North Caroline, p. 291.

[34] Schmutz, B., 2006. "A CFD guideline to simulate the flow around an airfoil".

[35] Boeuf, J.P., Lagmich, Y., Unfer, Th., Callegari, Th., and Pitchford, L.C., 2007. "Electrohydrodynamic force in dielectric barrier discharge plasma actuators" Journal of Applied Physics, 40 (), pp. 652-662.